Electronic Supplementary Material (ESI) for Catalysis Science & Technology.

Supplementary Content for:

Carbon-Supported Gas-Cleaning Catalysts Enable Syn Gas Methanation At Atmospheric Pressure

Meherzad F. Variava,* Tamara L. Church, Nikan Noorbehesht, Andrew T. Harris and Andrew I. Minett*

S1. Purification of MWNTs

Typically, as-synthesized MWNTs (200 mg) were added to $H_2SO_4(aq)$ (20 mL, 5 M) in a PTFE-lined microwave transparent pressure vessel. The vessel was transferred to a multimode microwave (MDS-10, Sineo) for digestion (20 °C min^{-1} to 220 °C, 20 min hold, 1000 W). The products were then filtered through an ethanol-wetted, 0.5-µm PTFE membrane (Millipore), washed with deionized (DI) water until the rinse water reached pH 7 (pH strips, LIVINGSTONE), and dried in a vacuum oven (120 °C, 24 h). The purified MWNTs were analysed using transmission electron microscopy (TEM) and thermogravimetric analysis (TGA).

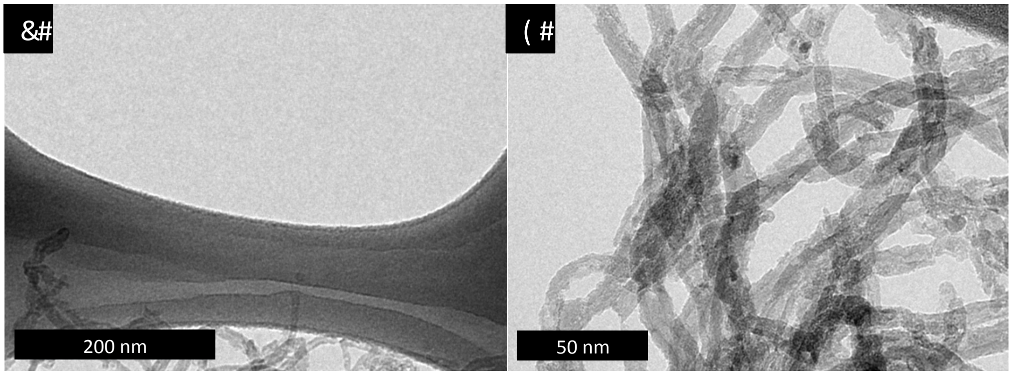

Figure S1. (A), (B) TEM of purified MWNTs.

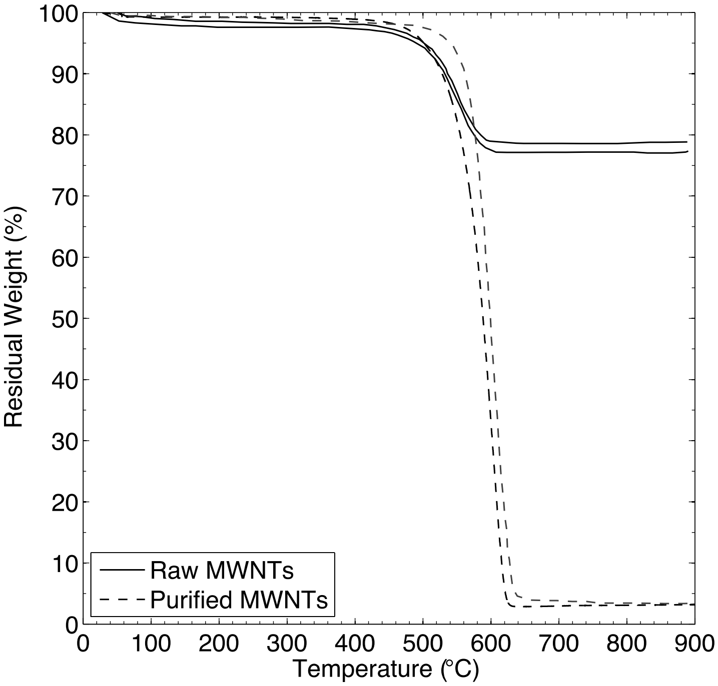

Figure S2. TGA of MWNTs (50 sccm instrument air, 5 °C min^{-1}).

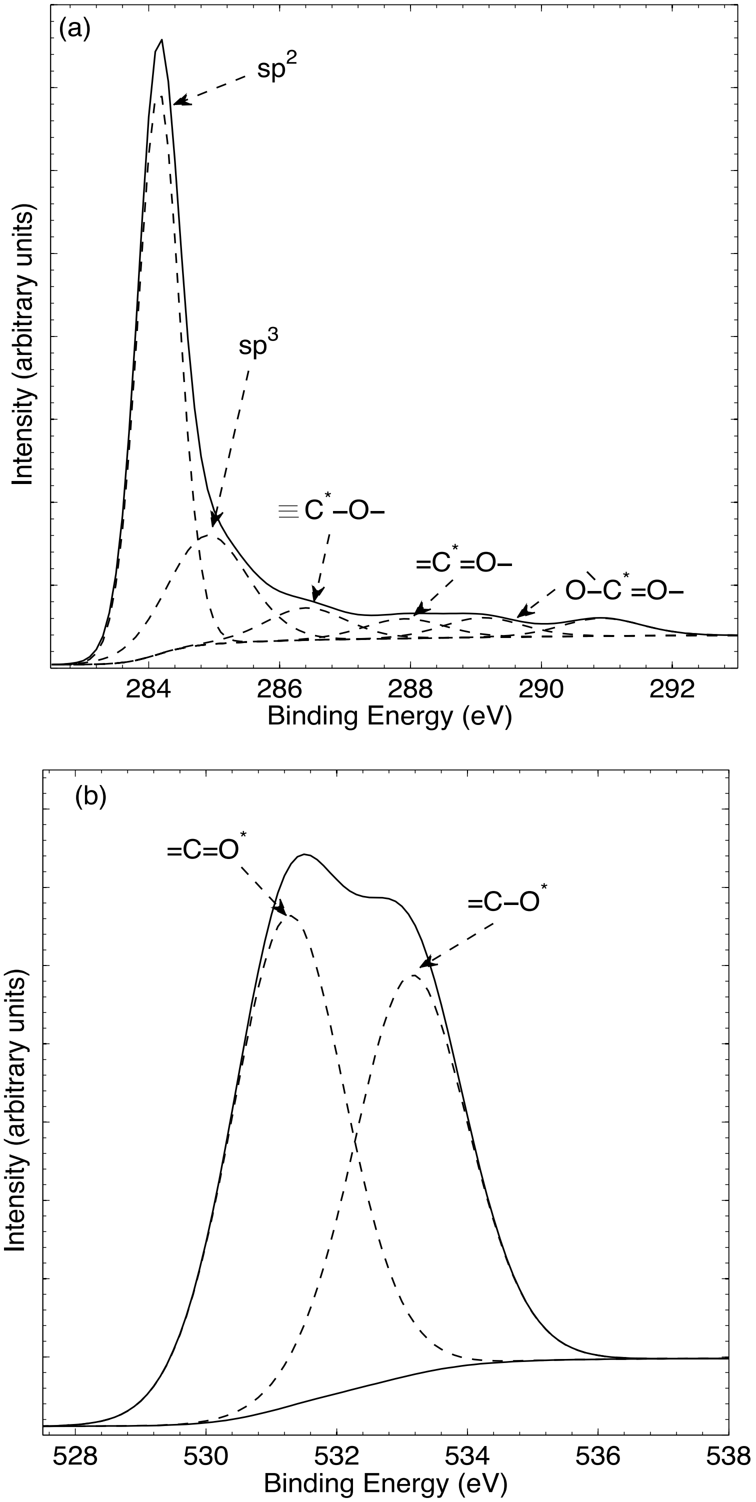

Figure S3. Deconvoluted X-ray photoelectron spectra of the purified MWNTs in the (a) C 1*s* and (b) O 1*s* regions.

S2. Characterization of MWNTs

For thermogravimetric analysis (TA SDT Q600), a quantity of sample (~10 mg) was heated (5 °C min^{-1}, 1000 °C) under instrument air (50 sccm). For transmission electron microscopy (TEM), 13Ni/MWNTs (~10 mg) were added to ethanol (15 mL) and the mixture was sonicated using a Branson Sonifier 450 tip sonicator (max power = 400 W, 10 min). Several droplets of the resulting mixture were dropped onto a holey carbon film, supported on a 200-mesh copper grid, and dried in air prior to analysis in a TEM (CM120-Biofilter (Philips), 120 kV). The crystalline structures of the synthesized catalysts were evaluated by X-ray diffraction (XRD, 2θ = 20–75°, interval = 0.0016°, dwell = 10 s) using Cu Kα radiation (λ = 0.1542 nm, SIEMENS D5000). The crystallite size was calculated via the Scherrer Equation (Equation S1),[1]

$$\tau = \frac{B\lambda}{\beta.\cos\vartheta} \qquad \text{(S1)}$$

where λ, B, ϑ, β, and τ are the wavelength of the X-rays used, shape factor (dimensionless, ≈ 0.94), Bragg angle, full width at half maximum (FWHM) of the peak in an XRD pattern and the mean size of the crystalline particle, respectively. Raman spectra were recorded (InVia, Renishaw) using an Ar^+ ion laser (λ = 514.5 nm). X-ray photoelectron spectroscopy (XPS) was carried out (ESCALAB250Xi, Thermo Scientific) using monochromatized Al Kα X-rays as the excitation source, and XPS-derived concentrations were calculated from detection-sensitivity-adjusted peak areas. To further verify the Ni loadings on the MWNTs, quantitative elemental analysis was performed using inductively coupled plasma–atomic emission spectrometry (ICP–AES, Vista AX, Varian). Briefly, NiO was extracted/dissolved from TGA oxidation residues by digestion in known volumes of Piranha solution (conc. H_2SO_4:H_2O_2 = 2:1, 40 °C, 3 h), further diluted to exactly 20 mL with DI water using a micropipette (100−1000 µL, VITLAB) and analysed at 230.078 nm. Final Ni concentrations were determined by comparing the resulting signal to a calibration curve (10 points) that was prepared using pre-diluted external standards (CHOICE Analytical). For temperature-programmed reduction with H_2 (H_2-TPR), the catalysts (~50 mg) were pretreated in an inert atmosphere (Ar, heated at 10 °C min^{-1} to 250 °C, hold 2 h) prior to analysis (3% H_2 in Ar, 60 sccm, 10 °C min^{-1}, 200–800 °C). The H_2 signal (mass units) was analyzed via the quadrupole mass spectrometer (MS; CIRRUS, MKS; 15 scans min^{-1}).

S3. Apparatus

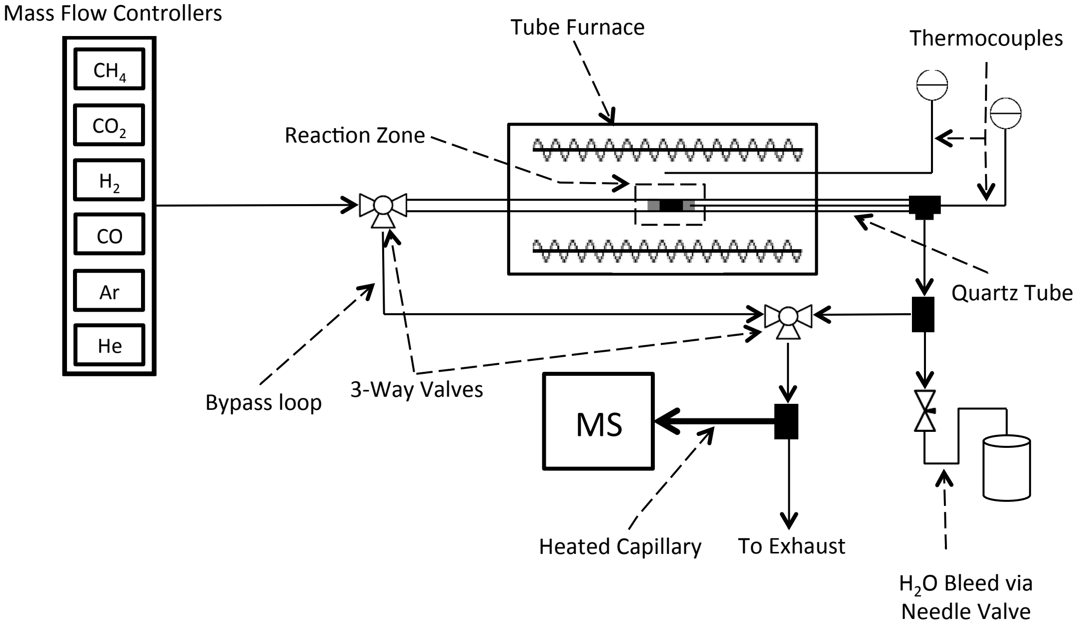

Figure S4. Schematic of the reactor unit for CO methanation through a bed of MWNTs-supported Ni catalysts. Within the "Reaction Zone", the catalyst bed (black) is supported on either side by quartz wool plugs (grey), which are in turn supported by two fingers (not shown) that were blown into the quartz tube during manufacture. Temperatures were recorded inside the quartz reactor as well as in the heated zone within the furnace (OTX-1200, MTI) and the difference ($T_{CatalystBed} - T_{HeatedZone}$) was ~5 °C. Gas flows were controlled using mass flow controllers (MFCs; Alicat Scientific). Further, even at high weight hourly space velocities (>32000 scc g_{cat}^{-1} h^{-1}), the pressure upstream of the catalyst bed was just above ambient (~15–16 psi). The needle valve was slightly open in order to bleed any water generated while keeping the system closed. H_2O generation was minimal due to the low overall reactant flow rates (37 sccm). Finally, for gas analysis, samples of the reactant and product gas streams (~13 sccm) were transferred via a heated capillary to the internally heated quadrupole mass spectrometer (MS) where 15–18 scans min^{-1} were collected. Note the presence of a bypass; this made pre-, mid- (every 3–6 h), and post-reaction calibrations, which are critical to reproducible quantitative analysis with quadrupole mass spectrometers, simple and fast.

S4. Interpretation of Mass Spectra

Table S1. Key gas species and corresponding ion fragments.

m/z	Key ion fragments	Represented species
2	H_2^+	Hydrogen
4	He^+	Helium
16	CH_4^{+}[a]	Methane
28	CO^{+}[a]	Carbon monoxide
44	CO_2^+	Carbon dioxide

[a] Contributions from CO_2 fragmentation to CO^+ and O^+ (m/z of 28 and 16, respectively) and CO fragmentation to C^+ and O^+ (m/z of 12 and 16, respectively), where applicable, were deducted (see Figure S6).

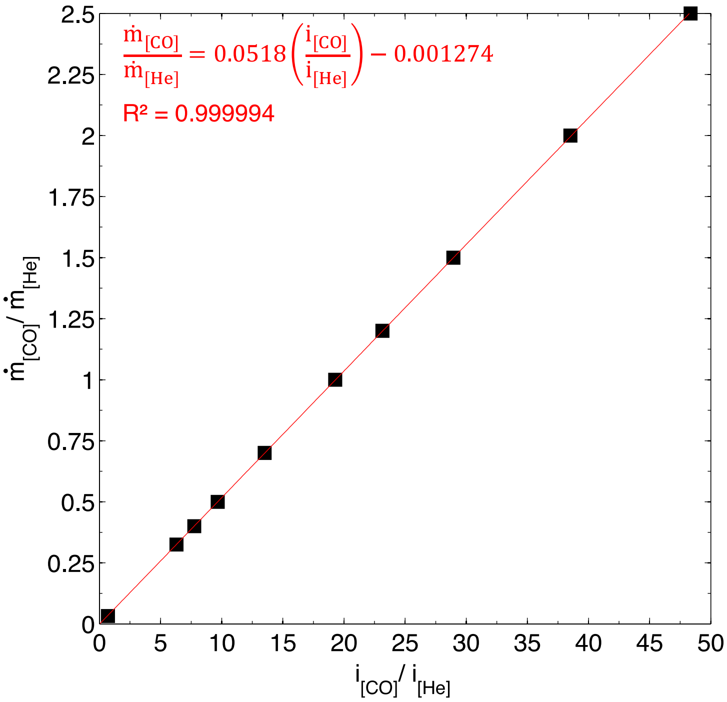

Figure S5. A sample ten-point [CO] calibration curve, where i (mass units) is the intensity of the species as recorded by the MS and $\dot{m}$ (sccm) is the standard mass flow of the particular gas, as set on the MFCs.

$$\dot{m}_{[gas]} = \left(\left(Sl \times {}^{i_{[gas]}}\!/_{i_{[He]}}\right) + Int\right) \times \dot{m}_{[He]}$$

Equation S2. The final mass flow $\dot{m}_{[gas]}$ (sccm), where i (mass units) is the intensity of the gases (as recorded by the MS), Sl and Int are the slope and intercept, respectively, of the calibration curve (Fig. S5), and $\dot{m}_{[He]}$ = 2 sccm is the flow rate of the internal standard.

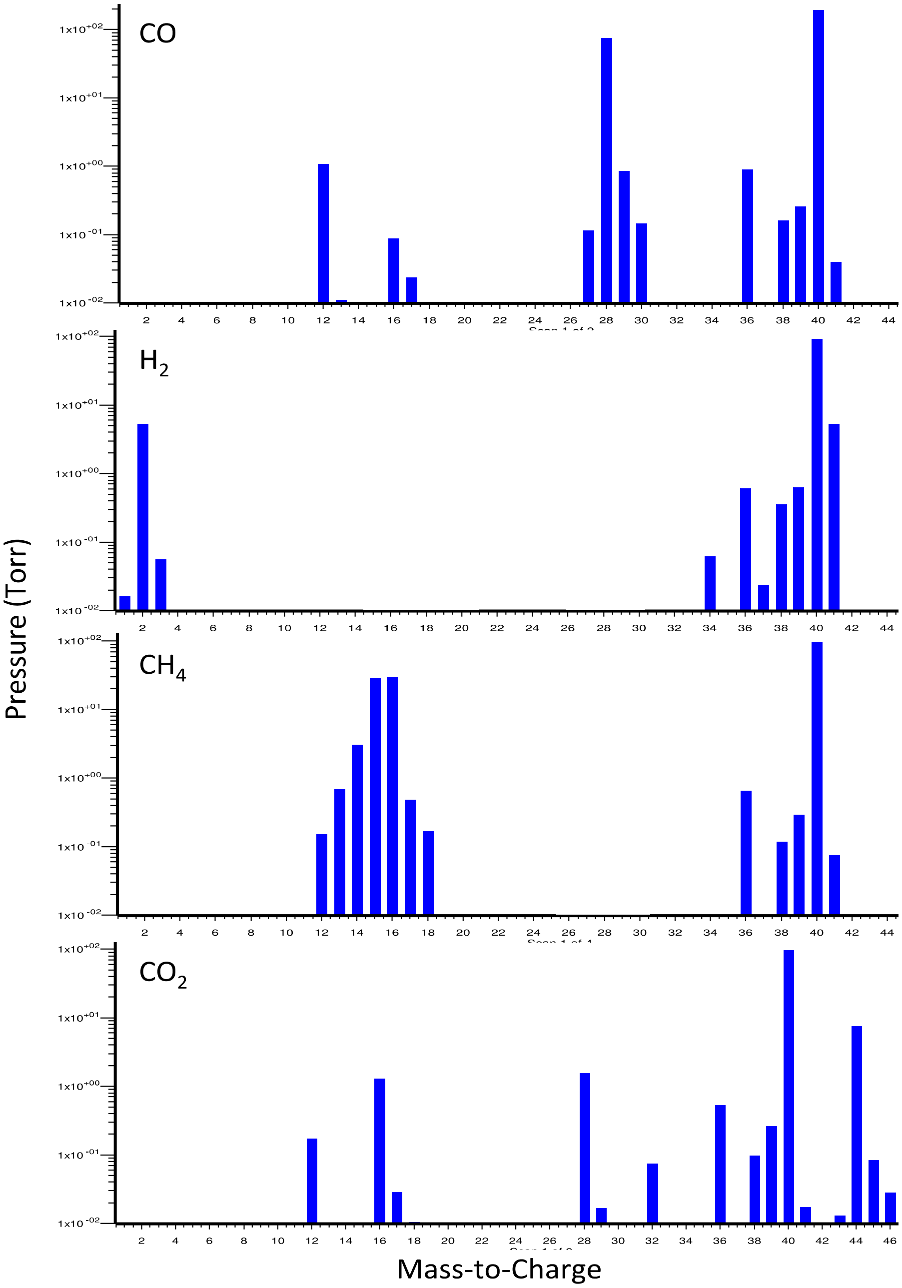

Figure S6. MS ionisation patterns of Ar-diluted CO (25%), H_2 (20%), CH_4 (30%) and CO_2 (5%).

S5. N_2 Adsorption-Desorption Isotherms

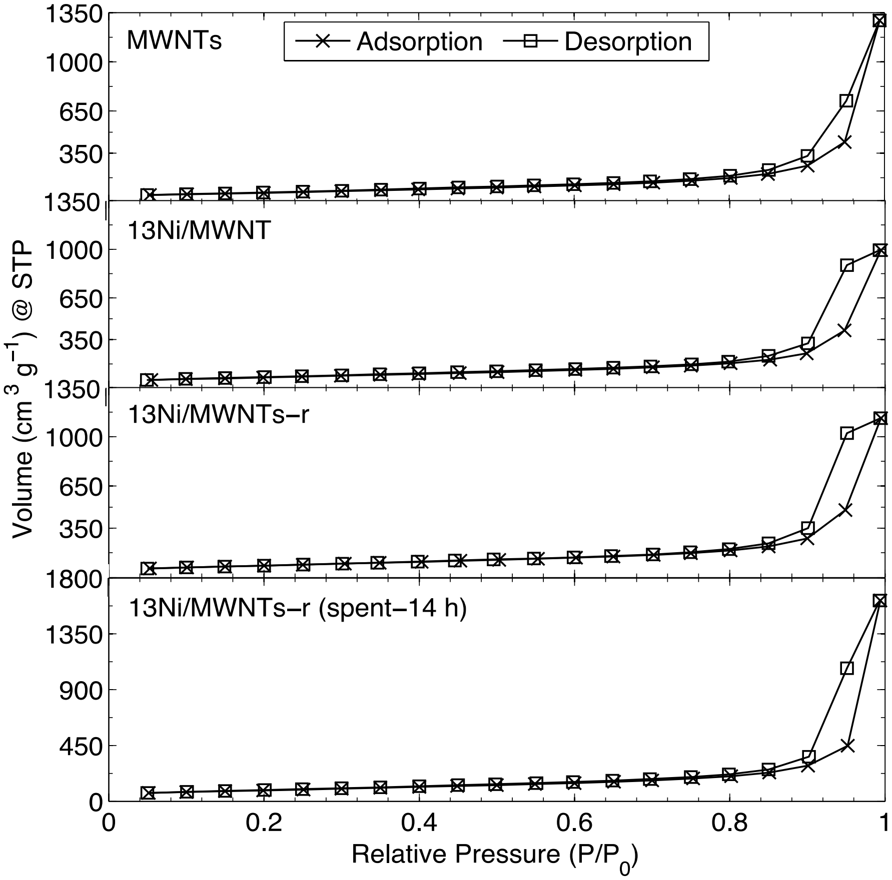

Figure S7. These N_2 adsorption-desorption isotherms, measured at −196 °C on a sorption apparatus (Autosorb-1, Quantachrome), were subsequently used to calculate the specific surface area (Brunauer–Emmett–Teller,[2] S_{BET}), pore size (Barrett–Joyner–Halenda,[3] BJH, adsorption branch), and pore volume of the catalysts.

S6. Raman Spectra

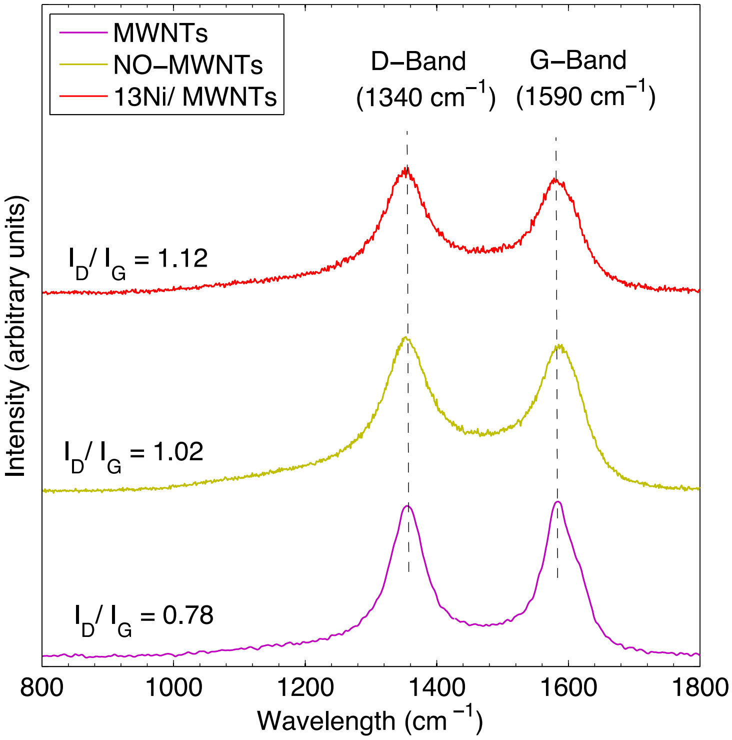

Figure S8. Raman spectra of MWNTs, NO-MWNTs and 13Ni/MWNTs. I_x = intensity of band x. Note, the D band at 1340 cm^{-1} is attributed to defects and the disorder within the walls of the MWNTs, and the G band at 1590 cm^{-1} is attributed to the C–C stretching mode of ordered graphitic carbon.[4]

S7. Thermogravimetric Analysis of 13Ni/MWNTs

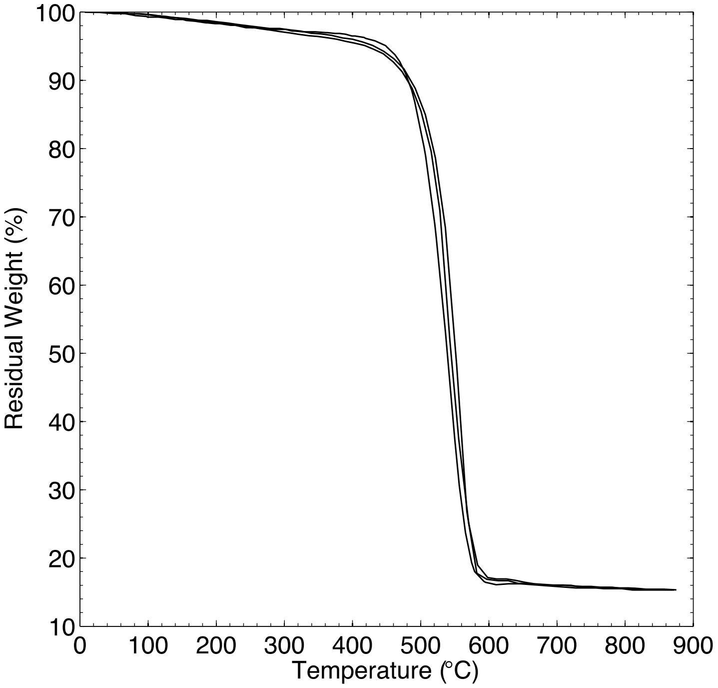

Figure S9. TGA of 13Ni/MWNTs (50 sccm instrument air, 5 °C min^{-1}).

S8. X-ray Photoelectron Spectroscopy of 13Ni/MWNTs

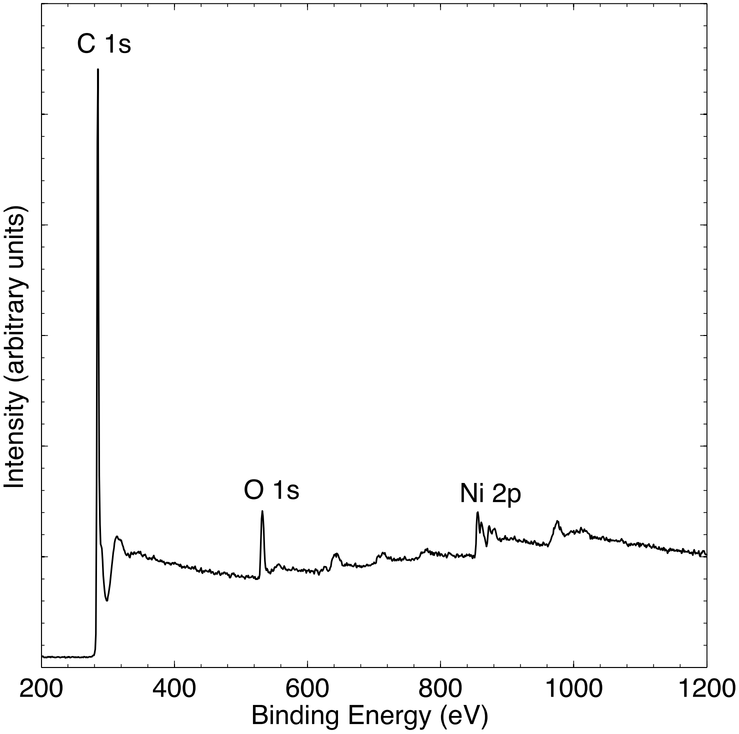

Figure S10. Survey XPS spectra of 13Ni/MWNTs catalysts.

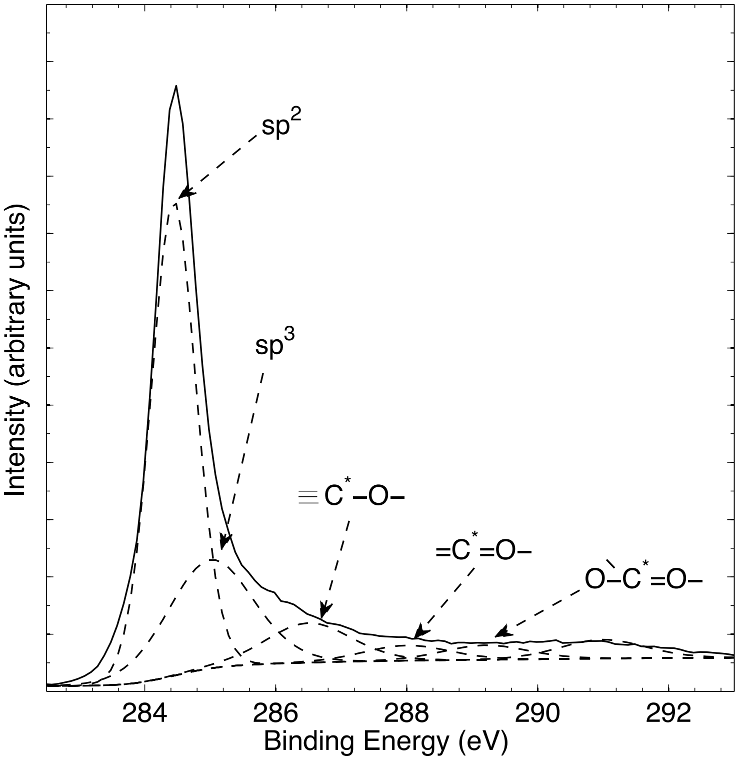

Figure S11. Narrow scan XPS of 13Ni/MWNTs in the C 1*s* region.

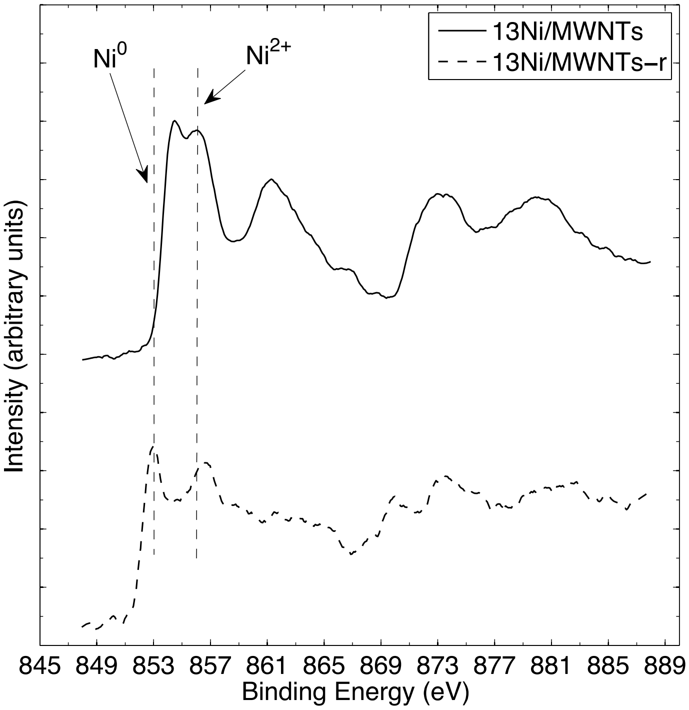

Figure S12. Ni $2p$ XPS spectra of 13Ni/MWNTs and 13Ni/MWNTs-r. Note the presence of the peak at 852.8 eV (for 13Ni/MWNTs-r), similar to the reported value for Ni^0.[5] However, a Ni^{2+} $2p_{3/2}$ peak at 856.4 eV was also present, likely formed from the exposure to air pre-analysis and/or from incomplete reduction. Note, the small difference between the BE values (<0.1 eV between the measured values and those reported for NiO) are within the range of variation caused by surface charge compensation.[6]

S9. Transmission Electron Microscopy Images of 13Ni/MWNTs

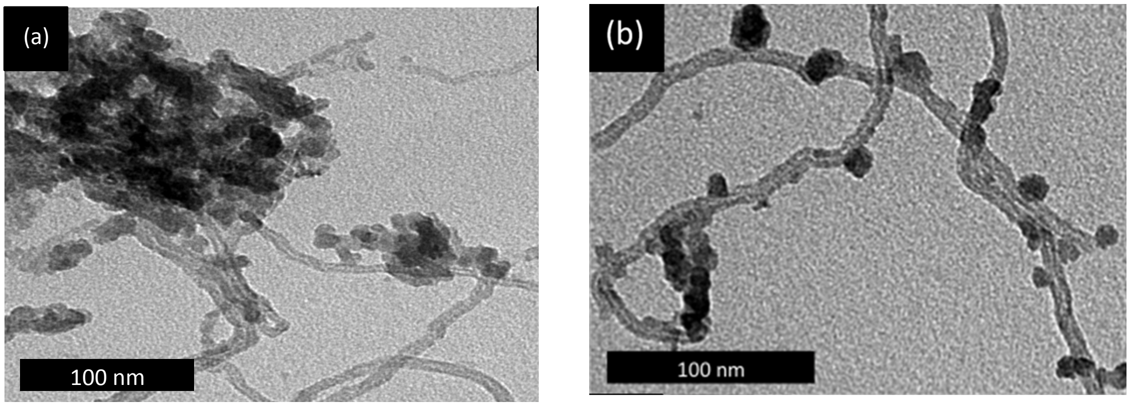

Figure S13. (a, b) Additional TEM images of the 13Ni/MWNTs.

S10. X-ray Diffraction Patterns

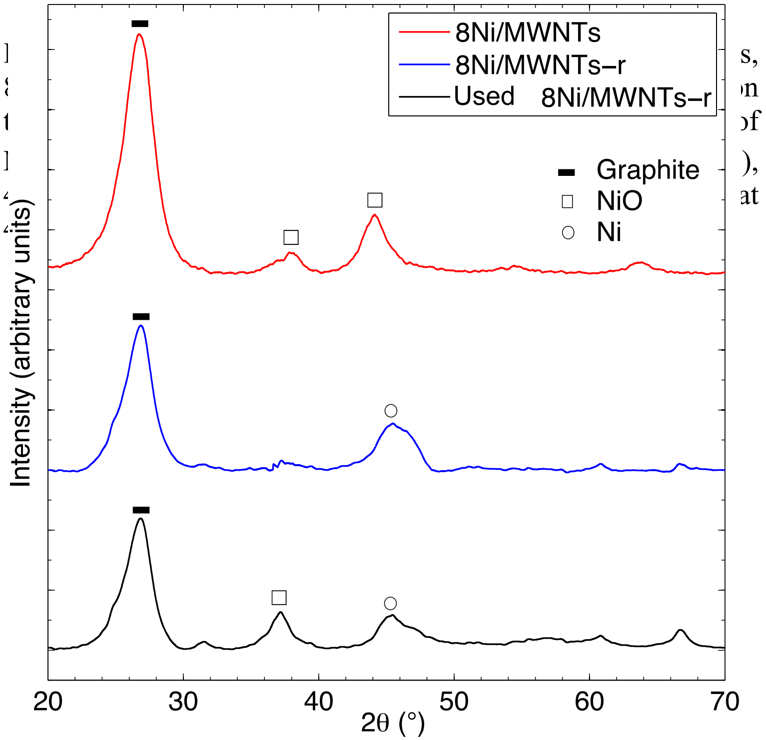

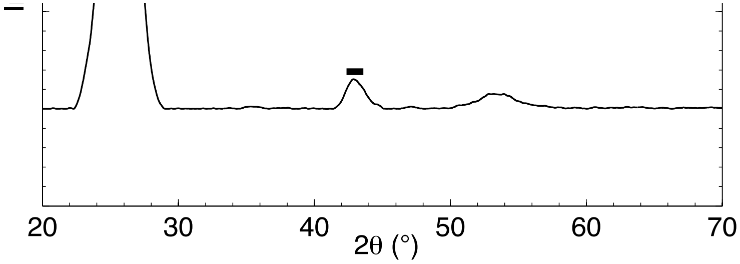

Figure S15. XRD pattern of NO-MWNTs. Indicated phase: (▬) the graphite structure (002) and (100) planes of MWNTs at 26.5° and 43.2°, respectively.

S11. H_2-based Investigations of MWNTs

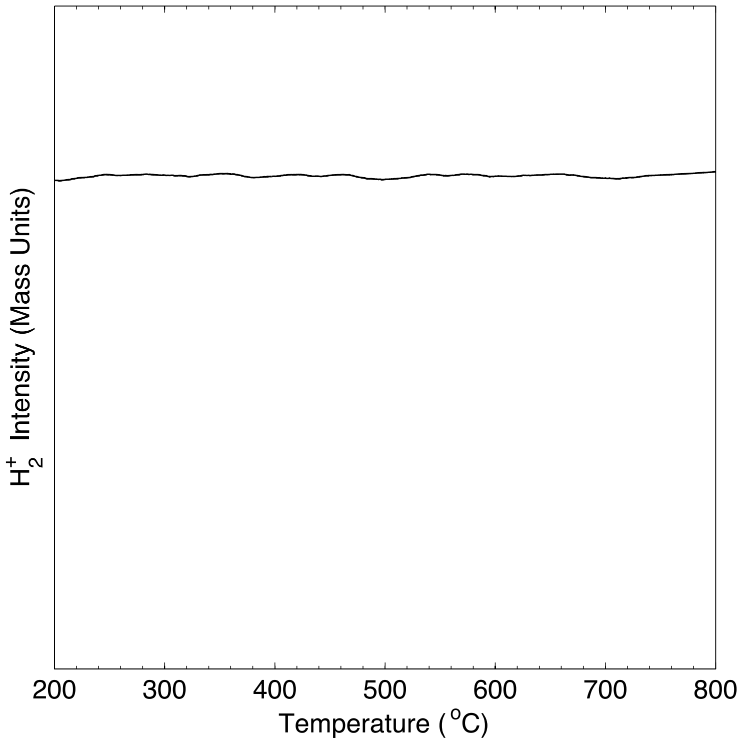

Figure S16. H_2-TPR of 13Ni/MWNTs-r. Analysis conditions: ~50 mg sample, 3% H_2 in Ar, 60 sccm, heated at 10 °C min^{-1} over 200–800 °C, sampled at 15 scans min^{-1}.

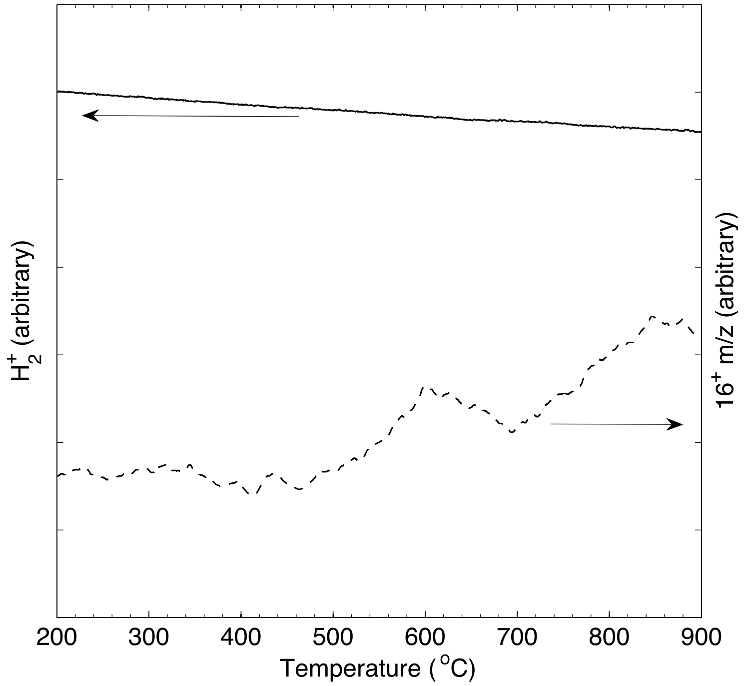

Figure S17. Effect of heating in H_2 (0.5%, bal. Ar, 35 sccm, d*T*/d*t* = 10 °C min^{-1}) on purified MWNTs (50 mg).

S12. Control Methanation Reactions

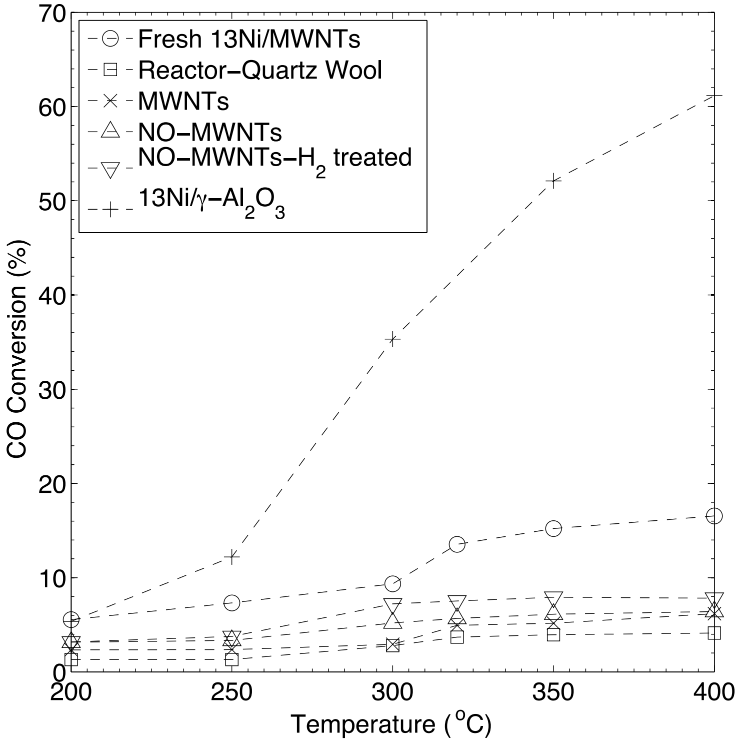

Figure S18. Control CO methanations. NO-MWNTs were synthesized by dispersing MWNTs in EtOH then drying and calcining in NO (0.1%, 3 h, 500 °C). MWNT-NO-H_2 treated was synthesized by annealing NO-MWNTs in H_2 prior to testing. 13Ni/γ-Al_2O_3, synthesized via incipient wetness impregnation and calcined in NO (as per *x*Ni/MWNTs synthesis, experimental section), was mixed with quartz wool, then reduced (10% H_2 in Ar, 50 sccm, 30 °C min^{-1} to 700 °C, hold 1 h). Reaction Conditions: total flow = 37 sccm ($CO/H_2/Ar$ = 1:3:3), ~70 mg of catalyst (when used). Conversion values were reported over 3 h of isothermal operation, except in the case of unreduced 13NiO/MWNTs, which was calculated after 15 min isothermal operation to avoid in situ reduction of the NiO).

S13. Thermodynamic Simulations

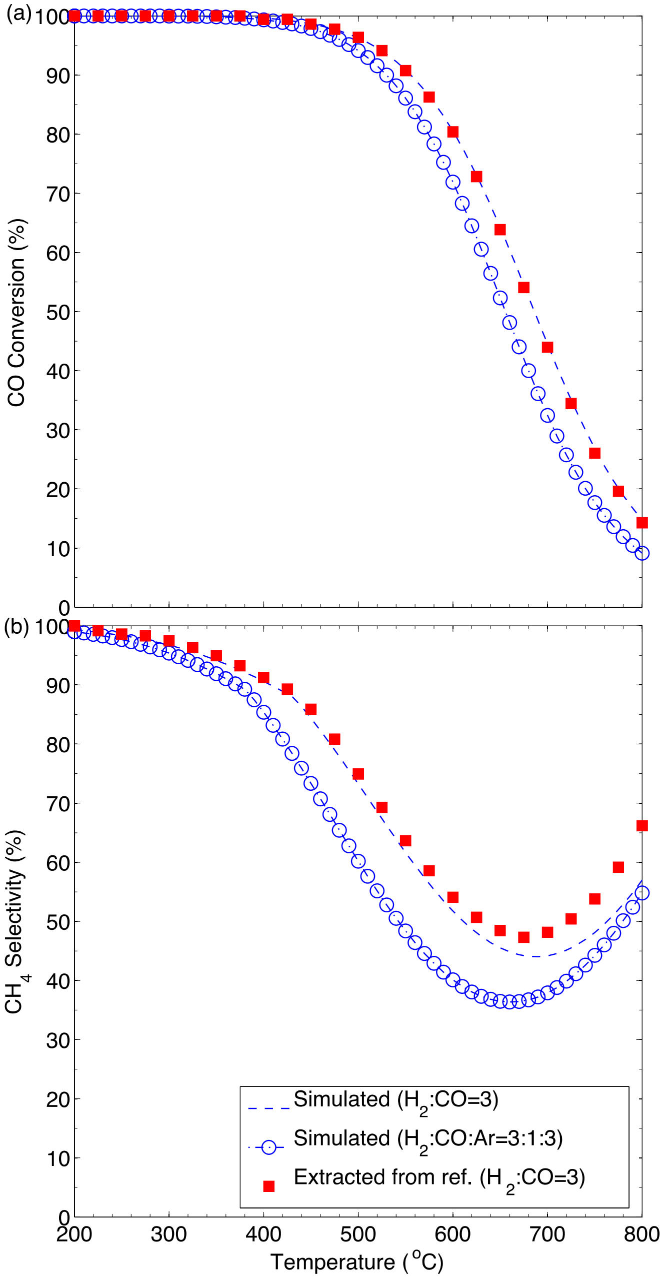

Figure S19. Thermodynamic simulations (Aspen Plus v7.3, Soave-Redlich-Kwong equations of state, Gibbs free reactor) starting from gas inputs from a previous report (---), and the current (○) gas composition used. Note, (■) denotes the extracted data points (GraphClick, Arizona Software) of thermodynamic simulations from Gao et al.,[7] for comparison with our developed model.

S14. Effect of Process Metrics

Weight-hourly space velocities (WHSVs), critical parameters for the large-scale industrial application of plug-flow catalysts,[8] were varied to ascertain the conversion and throughput limits of these catalysts (Figure S20). Conversions were maintained for WHSVs up to 40000 scc g_{cat}^{-1} h^{-1}; however, CO conversions were negligible at higher values and the catalytic effect was marginal, even when the temperature was raised to 400 °C. Thus, a WHSV of 32000 scc g_{cat}^{-1} h^{-1} was used, unless mentioned otherwise.

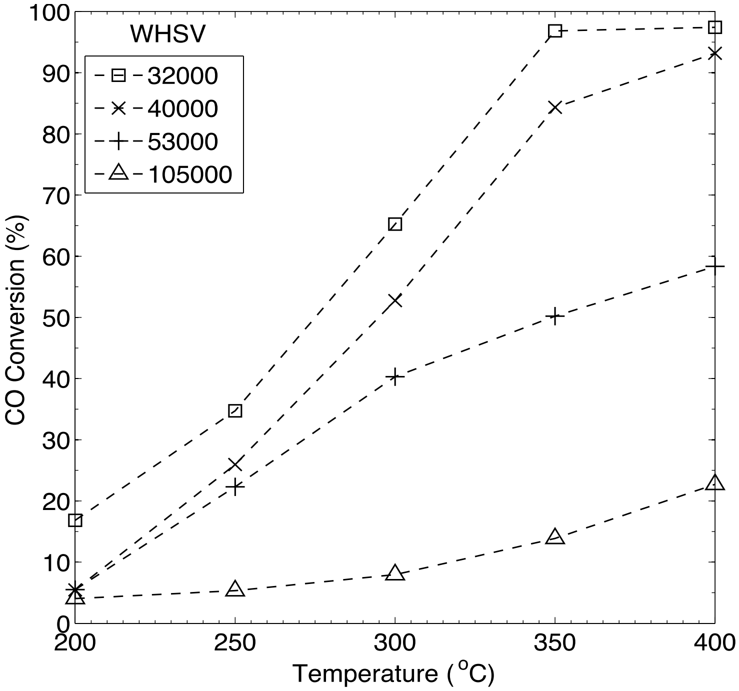

Figure S20. CO methanation over 13Ni/MWNTs at various WHSV values (scc g_{cat}^{-1} h^{-1}). Experimental details: catalysts (70 mg) were reduced (550 °C, 10% H_2 in Ar, 50 sccm, 60 min) and cooled (Ar, 65 sccm) to reaction temperature prior to introducing the reactants (13.5% CO, 41% H_2, 2 sccm He and balance Ar, total flow = 37 sccm). Values reported are after 5 h isothermal operation. WHSVs were altered by adjusting the amount of catalyst used.

The H_2/CO ratio (HCOR) in synthesis gas varies from one to eight, depending upon the feedstock and operating efficiencies of downstream gas-conditioning reactors (such as water−gas shift reactors).[9] The ideal HCOR for SNG synthesis from CO is ~3; we, however, tested the resilience of our catalysts to practical fluctuations that may occur and impact the equilibria described (Equations 1 and 3 within the manuscript). Although a low HCOR (i.e. <3) can generally be increased using a water−gas shift reactor unit (Equation S3), both H_2-poor and H_2-rich conditions were investigated to test the applicability limits of the catalyst.

$$CO + H_2O \rightleftharpoons H_2 + CO_2 \qquad \text{(S3)}$$

The effect of the HCOR variations is illustrated in Figure S20. The CO conversion was not significantly changed when the HCOR was increased from 3 to 5 (Figure S21). However, a higher HCOR enhanced the selectivity of the CO conversion to CH_4, which reached ~90% for HCOR = 5 (Figure S21). These observations were consistent with previous research,[7] where increased CH_4 selectivity was found by increasing the HCOR. However, at a lower HCOR (HCOR = 1 i.e. Equation S3), CO conversion reaches a maximum of ~65%, though the CH_4 selectivity does not exceed ~43%. Thus, although it is possible to generate CH_4 within a wide range of HCORs, high CH_4 yields can only be realised when HCOR is greater than 3.

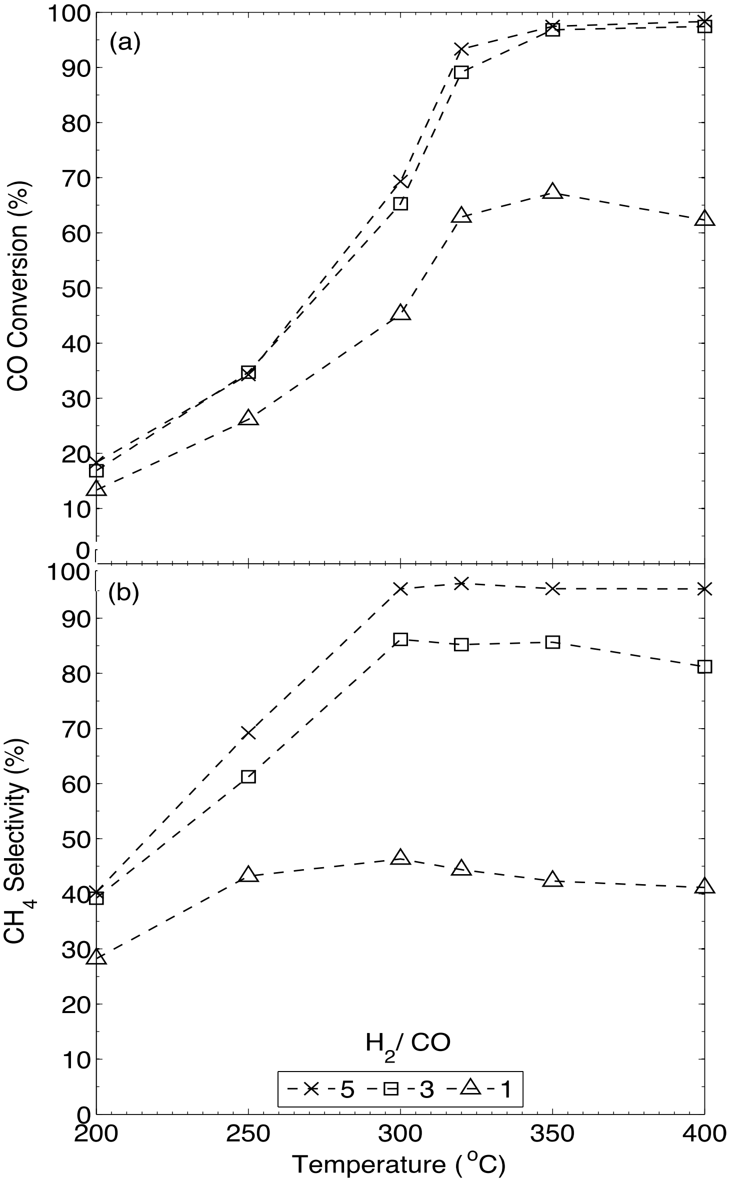

Figure 21. Effect of H_2/CO ratio on (a) conversion and (b) CH_4 selectivity of CO methanation over 13Ni/MWNTs-r. Experimental conditions: catalysts (70 mg) were reduced (550 °C, 10% H_2 in Ar, 50 sccm, 60 min) and cooled (Ar, 65 sccm) to reaction temperature, prior to introducing the reactants (13.5% CO, variable% H_2, 2 sccm He and balance Ar, total flow = 37 sccm). Values reported are after 5 h isothermal operation. H_2/CO ratios were varied by altering the H_2 and Ar (balance) flows while keeping the total gas flow at 37 sccm.

S15. Characterisation and Regeneration of Spent Catalysts

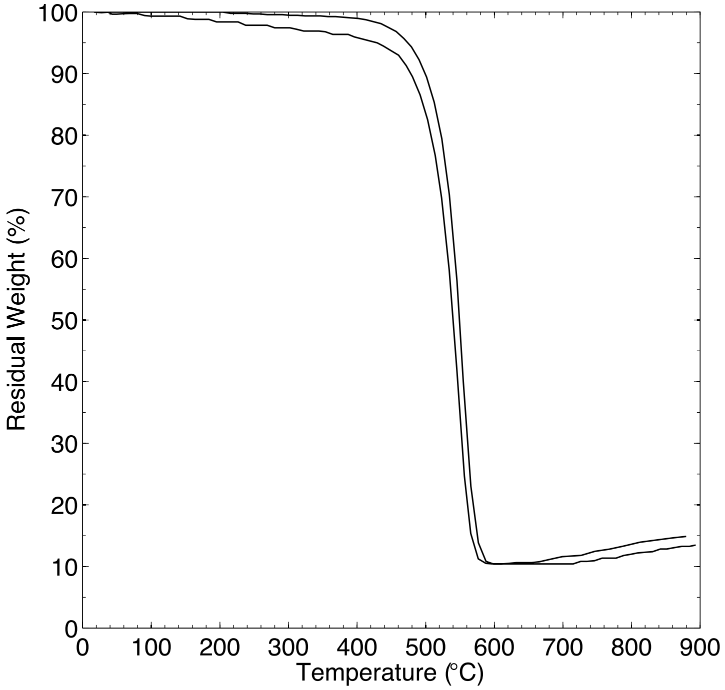

Figure S22. Thermogravimetric analyses (TGA) of 13Ni/MWNTs-r after use in a 150-h CO methanation at 350 °C in a fixed-bed CVD-type system. Analysis was performed under 50 sccm instrument air, d*T*/d*t* = 5 °C min^{-1}.

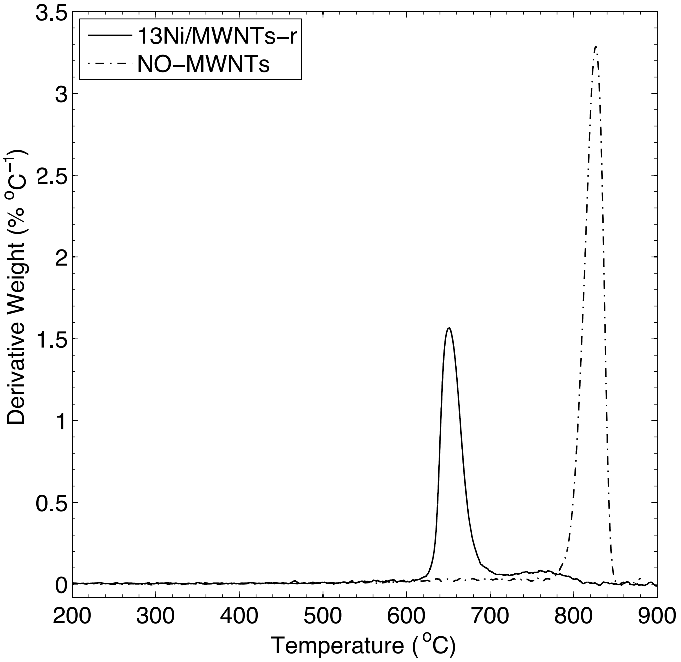

Figure S23. Thermogravimetric analyses (TGA) in a CO_2 atmosphere (30% in Ar, ramp at 5 °C min^{-1}). 13Ni/MWNTs-r were synthesized by treating 13Ni/MWNTs in a reducing atmosphere (10% H_2 in Ar, 550 °C, 50 sccm for 60 min); NO-MWNTs were dispersed in EtOH then dried and calcined in NO (0.1%, 3 h, 500 °C).

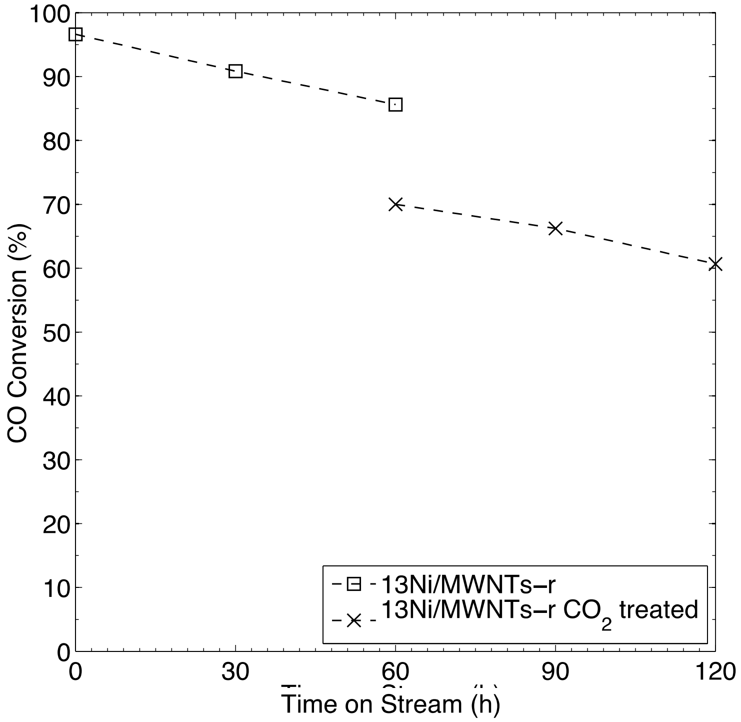

Figure S24. CO methanation performance of 13Ni/MWNTs-r and CO$_2$-treated (10%, in Ar for 40 min at 550 °C) 13Ni/MWNTs-r catalysts after 60 h. Experimental conditions: catalysts (70 mg) were reduced (550 °C, 10% H$_2$ in Ar, 50 sccm, 60 min) and cooled (Ar, 65 sccm) to 350 °C prior to introducing the reactants (13.5% CO, 41% H$_2$, 2 sccm He and balance Ar, total flow = 37 sccm).

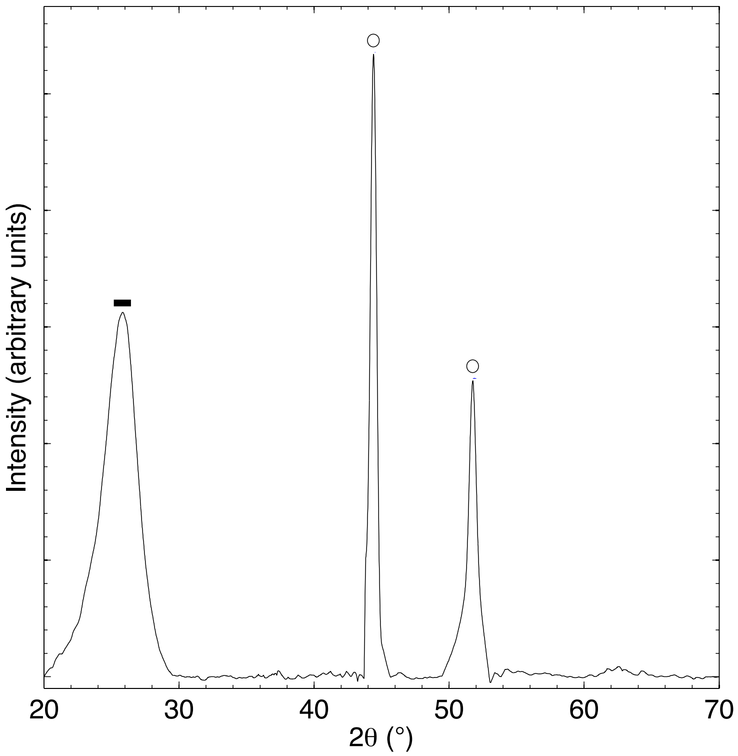

Figure S25. X-ray diffraction pattern of 13Ni/MWNTs that were subjected to a H_2 atmosphere (10% H_2 in Ar, 50 sccm, T = 550 °C) for an extended period (t = 5 h). Indicated phases are: (▬) graphite plane (002) of MWNTs at 26.5°; (o) Ni (JCPDS 45-1027) at 44.8° (111) and 51.8° (200).

S16. References

1. P. Scherrer, *Göttinger Nachr. Math. Phys.*, 1918, **2**, 98-100.
2. S. Brunauer, P. H. Emmett and E. Teller, *J. Am. Chem. Soc.*, 1938, **60**, 309-319.
3. E. P. Barrett, L. G. Joyner and P. P. Halenda, *J. Am. Chem. Soc.*, 1951, **73**, 373-380.
4. (a) S. Osswald, M. Havel and Y. Gogotsi, *J. Raman Spectrosc.*, 2007, **38**, 728-736; (b) M. S. Dresselhaus, G. Dresselhaus, R. Saito and A. Jorio, *Phys. Rep.*, 2005, **409**, 47-99; (c) S. Costa and E. Borowiak-Palen, *Acta Phys. Pol., A*, 2009, **116**, 32-35.
5. T. Hou, L. Yuan, T. Ye, L. Gong, J. Tu, M. Yamamoto, Y. Torimoto and Q. Li, *Int. J. Hydrogen Energy*, 2009, **34**, 9095-9107.
6. (a) B. L. Maschhoff and N. R. Armstrong, *Langmuir*, 1991, **7**, 693-703; (b) C. S. Kuivila, J. B. Butt and P. C. Stair, *Appl. Surf. Sci.*, 1988, **32**, 99-121.
7. J. Gao, Y. Wang, Y. Ping, D. Hu, G. Xu, F. Gu and F. Su, *RSC Adv.*, 2012, **2**, 2358-2368.
8. Z. Liu, B. Chu, X. Zhai, Y. Jin and Y. Cheng, *Fuel*, 2012, **95**, 599-605.
9. (a) R. M. Navarro, M. A. Peña and J. L. G. Fierro, *Chem. Rev.*, 2007, **107**, 3952-3991; (b) Y. Richardson, J. Blin and A. Julbe, *Prog. Energy Combust. Sci.*, 2012, **38**, 765-781.